Journal of Biophysical Chemistry, 2026, 17(4), 69-90
https://www.scirp.org/journal/jbpc
ISSN Online: 2153-0378
ISSN Print: 2153-036X

Copper (II) and Zinc (II) Complexes of Nicotinic Acid Hydrazide Derivative: Synthesis, Characterization, Density Functional Theory, Molecular Docking and Anti-Tubercular Studies

Ebobobi Ebotagbo[1], Evans Ngandung Mainsah[1], Gwendoline Mochia Toh-Boyo[1], Shintaro Suda[2], Natsuki Katsuumi[2], Terkumbur Emmanuel Gber[3,4], Offiong Efanga Offiong[4], Takashiro Akitsu[2*], Emmanuel Ngwang Nfor[1*]

[1]Department of Chemistry, Faculty of Science, University of Buea, Buea, Cameroon
[2]Department of Chemistry, Faculty of Science, Tokyo University of Science, Tokyo, Japan
[3]Computational and Bio-Simulation Research Group, University of Calabar, Calabar, Nigeria
[4]Department of Pure and Applied Chemistry, Faculty of Physical Sciences, University of Calabar, Calabar, Nigeria
Email: *nfor.emmanuel@ubuea.cm, *akitsu2@rs.tus.ac.jp

How to cite this paper: Ebotagbo, E., Mainsah, E.N., Toh-Boyo, G.M., Suda, S., Katsuumi, N., Gber, T.E., Offiong, O.E., Akitsu, T. and Nfor, E.N. (2026) Copper (II) and Zinc (II) Complexes of Nicotinic Acid Hydrazide Derivative: Synthesis, Characterization, Density Functional Theory, Molecular Docking and Anti-Tubercular Studies. *Journal of Biophysical Chemistry*, **17**, 69-90.
https://doi.org/10.4236/jbpc.2026.174005

Received: August 10, 2026
Accepted: September 25, 2026
Published: September 28, 2026

Abstract

A nicotinic acid hydrazide derivative $C_{15}H_{12}N_4O$(L1), its copper (II) and zinc (II) complexes ($[Cu(L1)_2]Ac_2$ and $[Zn(L1)_2]Ac_2$ respectively) have been synthesized. The prepared ligand L1 and it metal (II) complexes were characterized by melting point determination, elemental analysis, infrared spectra and ^{1}H-NMR spectroscopic techniques. In addition, the crystal structure of the L1was determined by single-crystal X-ray diffraction techniques. On the basis of the experimental and computational results, a tetrahedral geometry was proposed for the copper complex and distorted tetrahedral geometry for the zinc complex, consisting of two *NO*-donor atoms from the hydrazide ligand. The Hirshfeld surface analysis of the ligand was determined to verify the intermolecular interactions. The antibacterial activity of the free ligand and its Cu (II) and Zn (II) complexes was evaluated against *Mycobacterium tuberculosis*. The copper (II) complex showed promising result as antibacterial agents for *M. tuberculosis*, which with MIC value of 1.25 ± 0.13 μg/mL ± SD as compared to the standard drug with MIC value of 3.12 ± 0.34 μg/mL ± SD. Furthermore, molecular docking analysis was performed and the average binding energy of $[Cu(L1)_2]Ac_2$ with *M. tuberculosis* strain was extremely favourable (−8.3 kcal/mol), followed by the $[Zn(L1)_2]Ac_2$ complex with average binding energy of −7.8 kcal/mol as compared to that of the standard drug (−4.2 kcal/mol). These results revealed that, the complexes are potential candidates for the development of new antibacterial drug.

Keywords

Nicotinic Acid Hydrazide, Antitubecular Activity, DFT Calculations, Molecular Docking, X-Ray Cystallography

1. Introduction

The continuous threats posed by infectious diseases to human health and the rapid development of multi-drug resistant microbial pathogens have aroused serious global health concerns [1] [2]. It is anticipated that the formidable challenge posed by increased antimicrobial resistance to known clinical drugs might results to approximately 10,000,000 deaths by the year 2050 [2] [3]. The World Health Organization (WHO), has flagged an urgent global action plan calling for all countries to take measures against drug-resistant microbes and work towards the discovery of safe and efficacious new antimicrobial drugs with different mechanisms of action from those of well-known antimicrobial agents [4]-[7].

The *Mycobacterium* genus currently has more than 170 species that are environmental organisms known as non-tuberculous *Mycobacteria*, especially *M. avium* and *M. kansasii*. These organisms can cause respiratory disorders associated with chronic tuberculosis, bronchiectasis, and cystic fibrosis in humans [8]. These infections are considered a worldwide public health problem due to their complexity and long treatments duration, based on the combined administration of rifampicin, isoniazid, pyrazinamide and ethambutol, which already have resistant isolates [9] [10]. *Mycobacterium tuberculosis* has attracted the attention of researchers for being the causative agent of tuberculosis (TB), a disease which mainly affects the lungs and is transmitted through the air.

Zinc and copper ions have been reported to modulate enzymes activities, oxidative-reductive processes, catalytic and regulatory functions [11] [12]. Zinc has a specific role in bioinorganic processes because of the peculiar properties of its coordination compounds which can easily be four-, five- or six-coordinate, without a marked preference for six coordination [12]. The most studied metalloproteins in which zinc serves a structural role belong to the zinc-finger family, which is involved in control of nucleic acid replication, transcription and repair [13]. In zinc-finger proteins, zinc is tetrahedrally coordinate to histidines and/or cysteines, the coordination of aspartic acid and glutamic acid residues to the metal, also has been reported in metalloenzymes [14].

On the other hand, copper(II) complexes offer various potential advantages as antimicrobial, antiviral, anti-inflammatory, antitumour agents, enzyme inhibitor, chemical nucleases, and they are also beneficial against several diseases like copper rheumatoid and gastric ulcers [15] [16]. The choice of copper as the metal centre for drug design brings in features such as its redox chemistry versatility in addition to the production of a ROS-based mechanism of action and its less toxic nature. Therefore, the design of antibacterial compounds by combining an aromatic

heterocyclic organic fragment with a metal ion appears to be a good strategy for modern drug development. Such molecules may offer unique mechanism of action, multiple targets, reactive oxygen species generation, and prevention of acquired resistance and decreased toxicity, features which are often hard to achieve with purely organic structures [17]. Inspired by these and in continuation with our studies on the biological activities of metal complexes of aroylhydrazones compounds [18]-[21], we therefore report the synthesis, structural characterization, anti-tubercular, density functional theory and molecular docking studies of zinc (II) and copper (II) complexes of a new nicotinic acidhydrazide (an anti-tubercular drug) derivative.

2. Experimental

2.1. Materials and Methods

Nicotinic acid hydrazide, indole-3-carboxaldehyde, $Cu(CH_3OO^-)_2{\cdot}H_2O$ and $Zn(CH_3OO^-)_2{\cdot}2H_2O$ and analytical reagents grade chemicals and solvents were obtained commercially and used without further purification. Elemental analyses were performed in a PerkinElmer 2400 Series II CHNS/O micro analyzer. Infrared spectra (FT-IR) were obtained *via* a PerkinElmer FT-IR frontier single range–MIR spectrophotometer equipped with an attenuated total reflectance sample holder and diamond crystal. The spectra were recorded in the range of 4000 - 400 cm^{-1}. ^{1}HNMR spectra were recorded on a Varian Unity plus 400 MHz instrument, while Jenway conductivity/TDS meter model 4510 was used to measure the molar conductivity of the 10^{-3} M metal complexes in DMF at room temperature. The Gouy's balance was used to measure the magnetic susceptibilities of the metal complexes after Pascal's constants and $Hg[Co(SCN)_4]$ was used to calibrate the changes in diamagnetism. UV-visible spectra were recorded using a Shimadzu UVmini-1240 spectrophotometer.

2.2. Synthesis of the Ligand

Synthesis of the ligand N'-((1H-indol-3-yl) methylene)nicotinohydrazide(L1)

Nicotinic acid hydrazide (0.27 g, 2 mmol) was added to indole-3-carboxaldehyde (0.29 g, 2 mmol) in 25 mL of ethanolic solution with three drops of glacial acetic acid added as catalyst. The resulting mixture was refluxed for five hours at a temperature of 70˚C with continuous stirring. The product was left to cool overnight, removed by vacuum filtration; the products was washed several times with water, ethanol, and diethyl ether and dried in a desiccator. Yellow crystals suitable for single crystal X-ray diffraction studies were obtained from the ethanolic filtrate after 30 days. Yield 86%, Melting point: 209˚C**,** $C_{15}H_{12}N_4O$, m/e 264.10, Elemental Analysis; *Found*; C, 68.17; H, 4.58; N, 21.20; O, 6.05, *Calculated:* C, 68.38; H, 4.69; N, 21.18; O, 6.02, mp 214˚C;IR (KBr) (υ, cm^{-1}): 3178 (NH), 1657 (CO), 1600 (C=N), 1575 (C=C);^{1}H NMR (400 MHz, DMSO-d6) δ: 7.13 - 8.76 (m, 7H, Ar-H + [nicotine ring]), 7.87 (s, 1H, indole-H), 8.63 (s,1H, CH=NNH), 9.09 (s, 1H, Nicotine [N=CH-CCO]), 11.56 (br.s, 1H,CONHN, exchangeable), 11.64 (br.s, 1H, NH-indole).

2.3. Preparation of the Complexes

2.3.1. Synthesis of the Cu(II) N′-((1H-indol-3-yl)methylene) Nicotinohydrazide Complex([Cu(L1)$_2$]Ac$_2$)

The Schiff base L1, (0.26 g, 0.5 mmol) was added to Cu(CH_3OO^-)2·H_2O (0.046 g, 0.25 mmol) in a 25 mL ethanolic solution. The resulting mixture was refluxed for 5 hours at a temperature of 80˚C with continuous stirring using a magnetic stirrer. The pale-yellow solution obtained was allowed to cool overnight, the products removed by filtration; washed with ethanol and stored in a desiccator. Yield 83%. Melting point:230˚C. IR υ (cm^{-1}): IR (KBr) (υ, cm^{-1}): 1605 (C=O), 1580 (C=N), 1456, 1225, 520 (Cu-O), 492 (Cu-N); *m*/*e* (%) 587.10, Elemental analysis for $C_{30}H_{24}CuN_8O_2$ (%): *Calculated* C 61.27, H 3.43, N 19.05, O, 5.44; *Found*: C 61.33, H 3.51, N 19.09, O 5.48. ^{1}H-NMR (400 MHz, DMSO-d_6, δ, ppm): 6.86 (m, 3H, Ar-H), 6.99 (s, J = 8 Hz, 2H, Ar-H), 7.12 (d, J = 8 Hz, 2H, Ar-H), 7.53 (t, J = 8 Hz, 2H, Ar-H), 7.61 (sbr, 3H, Ar-H), 7.82 (s, 2H, indole-H), 7.90 (d, J = 8 Hz, 1H, Ar-H), 8.25 (s, 1H, Ar-H), 9.04 (s, 2H, Nicotine [N=CH-CCO]) 10.81 (d, 2H, Ar-H), 11.60 (br.s, 2H, NH-indole), 11.97 (s, 2H, N-H).

2.3.2. Synthesis of the Zn(II)N′-((1H-indol-3-yl)methylene) Nicotinohydrazide Complex([Zn(L1)$_2$]Ac$_2$)

The Schiff base, L1, (0.26 g, 0.5 mmol) was added to Zn(CH_3OO^-)$_2$·2H_2O (0.046 g, 0.25 mmol) in a 25 mL ethanolic solution. The resulting mixture was refluxed for 5 hours at a temperature of 80˚C with continuous stirring using a magnetic stirrer. The pale-yellow solution obtained was allowed to cool overnight, the products removed by filtration; washed with ethanol and stored in a desiccator. Yield 89%. Melting point: 237˚C. ; IR (KBr)(υ, cm^{-1}): 1590 (C=O), 1540 (C=N), 1332, 1025, 540 (Zn-O), 481 (Zn-N), *m*/*e* (%) 588.1 (100); Elemental analysis for $C_{30}H_{24}ZnN_8O_2$ (%): Calculated C 61.08, H 3.42, N 18.99,O, 5.42; Found: C 61.23, H 3.45, N 19.01,O 5.46. ^{1}H-NMR (400 MHz, DMSO-d_6, δ, ppm): 6.97 (m, 3H, Ar-H), 6.99 (s, J = 8 Hz, 2H, Ar-H), 7.13 (d, J = 8 Hz, 2H, Ar-H), 7.40 (t, J = 8 Hz, 2H, Ar-H), 7.44 (sbr, 3H, Ar-H), 7.60 (d, J = 8 Hz, 1H, Ar-H), 7.81 (s, 2H, indole-H), 8.29 (s, 1H, Ar-H), 8.31 (d, 2H, Ar-H), 9.00 (s, 2H, Nicotine [N=CH-CCO]), 11.38 (s, 2H, N-H), 11.60 (br.s, 2H, NH-indole).

2.4. X-Ray Crystallography

Orange single crystals (plate-like with 0.952 × 0.685 × 0.264 mm^3 for L2) was served for analysis. The samples were set on top of a glass capillary, coated with a thin layer of Araldite epoxy resin. Intensity data were collected on a Bruker APEX2 CCD diffractometer (Bruker, Billerica, MA, USA) with Mo-Kα radiation monochromated by graphite (λ = 0.71073 Å) at 173. (2) K. Data treatment used the program package SAINT (Bruker, Billerica, MA, USA). An empirical absorption correction for intensity was applied by the program SADABS (Bruker, Billerica, MA, USA). In this program package, the structures (phase problem) were initially solved by direct methods with a SHELXS-97 [22], expanded by Fourier techniques, and finally refined by full-matrix least-squares methods based on F^2 using

a SHELXL-97 program [22]. All non-hydrogen (heavy) atoms were readily located to construct a model and were refined by anisotropic (thermal) displacement parameters. Hydrogen atoms were located at geometrically calculated positions and refined using riding models.

2.5. Hirshfeld Surface Study

The CRYSTAL EXPLORER [23] program was used for Hirshfeld surface analyses and fingerprint plots. The Hirshfeld surface was represented by the normalized contact distance (d_{norm}). If it is shorter than the van der Waals radius, it is shown in red, and if it is longer, it is shown in blue. In two-dimensional (2D) fingerprint plots, d_e was plotted on the vertical axis and d_i was plotted on the horizontal axis.

2.6. Density Functional Theory Study

The optimized geometry carried out on the ligand and its metal(II) complexes were modeled within the framework of density functional theory (DFT) with the help of Gauss View 6.0.16 and Gaussian09 suite of programs [24] [25]. Ground state energy of all the system was optimized in vacuum using the genECP methods by assigning the 6-311++G(d,p) and the SDD basis set for the lighter and heavier atoms respectively. The long-range corrected ωB97XD DFT functional was chosen for the complete calculations. The Highest occupied molecular orbital and lowest unoccupied molecular orbital (HOMO-LUMO) were computed at DFT/ωB97XD with /6-311++G (d,p). By invoking Gaussian 16W, natural bond orbital (NBO) analysis that utilizes the stabilization energy to study the magnitude of inter and intra molecular charge transfer between molecules were computed using the in-build Gaussian 3.1 method available in Gaussian 16W software. For this work TDOS, PDOS and OPDOS as well as the quantum theory of atoms in molecules (QTAIM) were computed using Multifunctional wavefunction analyze developed by Tian Lu's research group and downloaded from an official webpage (http://sobereva.com/multiwfnbbs) [26] in order to study the elements contributions to the molecular orbitals, and the strength and nature of the bonding concept herein.

2.7. Antibacterial Activity

The anti-tubercular activities of the ligand and its metal (II) complexes were assessed against *M. tuberculosis ATTC 27294* [27] using the micro plate Alamar Blue assay (MABA) [28]. This method is nontoxic, used as a thermally-stable reagent and shows good correlation with proportional and BACTEC radiometric methods [29] [30]. A standard solution containing 1000 ppm of each compound was prepared. From the standard solution, test solutions were prepared in the increasing concentration from 0.8 μg/mL to 100 μg/mL. In sterile 96 well plate, mixture of test solution, de-ionized water (200 μL) and middlebrook 7H9 Broth (100 μL), were taken. This plate was sealed and hatched at 37˚C over a period of five days. Further, 25 μL of Tween 10% and 80% and Almar Blue (1:1 ratio) was dis-

pensed in each well and incubated for one day. Minimum Inhibition Concentration (MIC) was reported as pink coloration for the growth of mycobacterium while blue coloration was considered as no bacterial growth in the well [31].

2.8. Molecular Docking

Molecular docking studies were performed using the Bio *via* discovery studio and auto dock vina tools [32]. The ligand L1 and its copper (II) and zinc (II) complexes were respectively sketched using Gauss View 6.0.16 [33] and later subjected to energy minimization. The log files from the optimized structure were then saved in PDB format for docking analysis. Bio *via* discovery studio was used in the preparation of the protein where water and other unwanted molecules were deleted, while polar hydrogen was added to the protein prior to docking. X -ray structure of Isoniazid with access number (DB00951) was downloaded from drug databank (DDB) as an Antibacterial agent used primarily as a tuberculostatic [34]. This remains a standard drug for treatment of tuberculosis and was used herein as a standard drug against the receptor protein 5e2c which was downloaded from RCSB (research Collaboratory for structural bioinformatics) powered by the protein data bank (PDB) (http://www.rcsb.org/pdb/home/home.do) [35] archives information about the shape of proteins and the nucleic acid. At therapeutic levels isoniazid is bactericidal against actively growing intracellular and extracellular *Mycobacterium tuberculosis* organisms. The mechanism of action of 5e2c prompted its usefulness in this study as a *Mycobacterium tuberculosis* protein. Pymol visualizer was used to visualize the docking result [36]. The interactions pictures were generated using the discovery studio visualize program.

3. Results and Discussion

The elemental analyses for C, H, N and O revealed that the calculated values for the Schiff base ligand L1 are in agreement with the experimental values, thus confirming the proposed molecular formula $C_{15}H_{12}N_4O$ for the ligand. The agreement between the calculated and experimental elemental analyses values for the metal complexes revealed a 1:2 (metal-ligand) stoichiometry, thus confirming their suggested formulae. These results further confirm the high purity of the Schiff base and its metal (II) complexes which were very soluble in DMSO and less soluble in methanol. They melted with decompositions at the temperatures of 209˚C, 230˚C and 237˚C for L1, $[Cu(L1)_2]Ac_2$ and $[Zn(L1)_2]Ac_2$ respectively.

3.1. Spectroscopic Analysis

The infrared spectra of the ligand L1 and its metal (II) complexes were recorded within the 4000 – 400 cm^{-1} region. The IR-spectrum of the hydrazone ligand exhibited a medium band at 3178 cm^{-1} attributed to ν(NH) stretching vibrations. The strong bands at 1657 and 1600 cm^{-1} in the spectrum of the ligand, corresponds to the presence of ν(C=O) [19] and ν(C=N) vibration modes [19]. Bands appearing at 995, 939, 800, and 781 cm^{-1} in the spectrum of L1 are the usual modes

of C-H of the aromatic ring vibrations and these revealed small shifts in the metal(II) complexes compared to the free ligand, which is the expected electronic structure changes that occur with coordination of the ligand to metal(II) ions. In the spectrum of the copper(II) complex, the ν(C=O) and ν(C=N)vibration bands experience negative shifts to 1605 cm^{-1} and 1580 cm^{-1}, respectively, compared to the ligand. This indicates the coordination the carbonyl oxygen and the azomethine nitrogen atoms to the copper(II) ion. In the low frequency region, the bands in the region 520 and 492 cm^{-1} are probably due to ν(Cu-O) and ν(Cu-N) vibrations, respectively. In the spectrum of the Zn(II)complex, the ν(C=O) and ν(C=N) vibration bands have also experienced a negative shift to the frequencies of 1590 and 1540 cm^{-1}, respectively, indicating coordination of the carbonyl oxygen and the azomethine nitrogen atoms to the Zn (II) ion. In the low frequency region, the bands in the regions 540 and 481 cm^{-1} are probably due to the ν(Zn-O) and ν(Zn-N) vibrations, respectively [37].

The structural features of the ligand and its metal (II) complexes in this investigation are supported by the ^{1}HNMR spectra obtained in DMSO-d_6 solution. In the ^{1}HNMR spectrum of the ligand, the multiplets at δ 7.13 - 8.76 ppm are attributed to the pyridyl rings protons. The amide proton is attributed to the signals at δ 9.19 ppm in the ligand. In the copper complex, the pyridyl ring protons are attributed to the signals at δ 6.86 - 10.81 ppm, with the amide proton attributed to the signal at δ 11.97 ppm. The zinc(II) complex also exhibited signals at between δ 6.97 - 8.31 ppm attributed to the pyridyl ring protons, while the amide proton further exhibited signal at δ 11.38 ppm. All the changes in the signals of the pyridyl ring, amide and methyl protons in the metal(II) complexes, suggests the involvement of the azomethine nitrogen and carbonyl oxygen atoms in coordination [37] [38].

3.2. Conductivity Measurements

The molar conductivity studies of the prepared compounds were evaluated to ascertain their electrolytic nature. They were first dissolved in DMF at room temperature at a concentration of 1.0×10^{-3} M. The conductivity of $[Zn(L1)_2]Ac_2$ and $[Cu(L1)_2]Ac_2$ was found to be 5.43 and 8.72 $\Omega^{-1}\cdot cm^2\cdot mol^{-1}$ respectively, which are low molar conductance values and could be attributed to their non-electrolytic nature [39].

3.3. UV-Visible Spectra and Magnetic Measurements

For the copper(II) complex, it exhibited two bands at 475 and 503 nm which are indicative of the tetrahedral geometry, assigned to the $^3T_1(F)\rightarrow{}^3T_2(\upsilon)$ and $^3T_1(F)\rightarrow{}^3A_2(\upsilon)$ [40]. The spectrum of zinc(II) complex exhibited a single band at 378 nm attributed to the charge transfer transition, which corresponds to the complex possessing tetrahedral structure [41]. For the magnetic measurements which was calculated in Bohr's Magnetons using the formula $\mu_{eff} = 2.83$ [(Xg x M.wt) – (diamagnetic correction)]$^{1/2}$ where Xg = complex's determine gram of magnetic

susceptibility. The calculated μ_{eff} value for nickel (II) complex was 3.73 BM supporting the tetrahedral geometry [40]. The zinc (II) complex on the other hand showed a diamagnetic character which could also be attributed to a tetrahedral geometry [41].

3.4. Crystal Structure of the Ligand (L1)

The molecular structure of L1 is depicted in **Figure 1(a)** along with the atomic numbering scheme. The crystal structure refinement data for L1 is given in **Table 1**. The L1 has two independent molecules having different torsion angles N3-N2-C6-O1 (−6.15), N2-C6-C5-C1 (20.37) and O1-C6-C5-C4 (18.34) in the asymmetric unit of the crystal designated as molecule A (green) having a planar structure, and the torsion angles of C22-C23-C26-C27 (−1.02), N7-N6-C21-O2 (0.78) and O2-C21-C26-C19 (−24.62) in the asymmetric unit of the crystal designated as molecule B (blue) with a twisted structure as in **Figure 1(b)**. These torsion angles values are essentially of interest in view of their close relation with the effects of embedding of ligand into the portion of the protein molecule. There are a total of 8 molecules of $C_{15}H_{12}N_4O$ in the unit cell. The Schiff base L1 crystallizes in the monoclinic system in space group $P2_1/c$. In L1, the bond distance C(21)-O(1) is equal to 1.236(3) Å indicating its double bond nature. The bond lengths N(6)-N(7) and C(21)-N(6) are equal to 1.392(3)Å and 1.342(3)Å, respectively while C(21)-N(6)-N(7) equal to 120.63(17) [39]. Most of bond distances and angles were within common ranges of normal covalent bonds. The intermolecular hydrogen bond between (indole) N4-H…O1 (carbonyl) was observed for L1 molecule (**Table 2**). The 6-membered aromatic rings are stacked *via* weak Π-interaction, and stacked rings of B are perpendicular to C=N bond of A.

Table 1. Crystal data and structure refinement of **L1**.

Empirical formula	$C_{30}H_{24}N_8O_2$
Formula weight	528.57
Temperature (K)	173
Crystal system	monoclinic
Space group	$P2_1/c$ (# 14)
a, (Å)	11.4069(18)
b, (Å)	12.822(2)
c, (Å)	18.149(3)
α (˚)	90.0000
β (˚)	94.810(4)
γ (˚)	90.0000
Volume (Å^3)	2645.1(7)
Z	4
ρ_{calc} (g/cm^3)	1.327
μ (mm^{-1})	0.088
F(000)	1104

Continued

Crystal size (mm^3)	0.12 × 0.11 × 0.1
Radiation	Mo Kα (λ = 0.71073)
T_{min}, T_{max}	0.93, 0.98
No. of reflections	5116
No. of parameters	362
Goodness of fit	1.127
$R_1[I > 2\sigma(I)]$	0.0367
WR_2	0.1040

Table 2. Prominent hydrogen bond distances (Å) and angles (˚).

D-H---A	H---A (Å)	D---A (Å)	D-H---A (˚)
Compound L1			
N(4)-H(4)---O(1)	2.808(4)	3.688(5)	24.87(1)
N(1)-H(6)---N(6)[a]	0.880(4)	3.032(5)	8.84(2)
O(2)-H(2A)---N(2)[b]	0.880(4)	2.882(5)	163.90(1)

D, donor; H, hydrogen; A, acceptor. Symmetry codes: (a) –x, -y, 2-z (b) −1/2 + x, 1/2 − y, −1/2 + z.

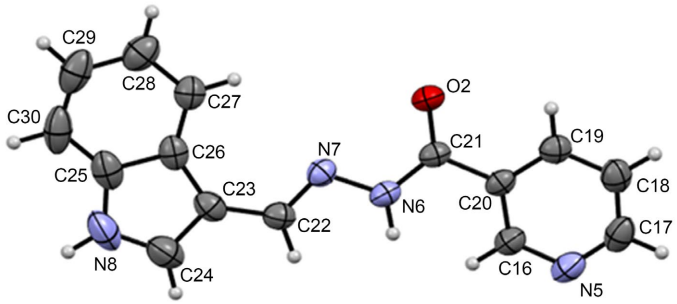

(a)

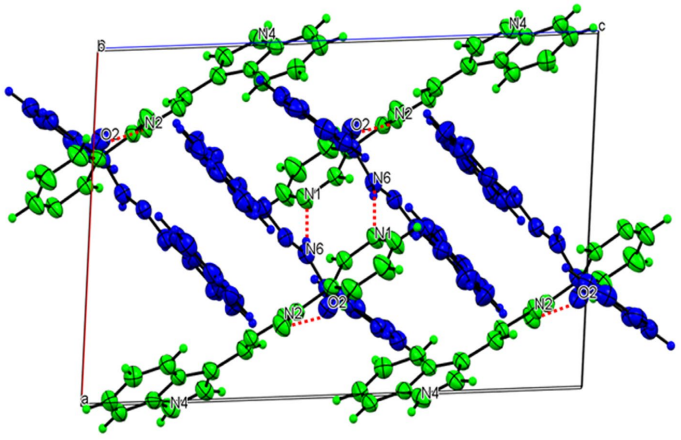

(b)

Figure 1. (a) Molecular structure with atom numbering scheme (b) Crystal packing of distinguished crystallographic independent molecules (A = green, B = blue) and molecular structures of for L1.

3.5. Hirshfeld Surface Analysis

In order to clearly understand the intermolecular interactions in L1, Hirshfeld surface analysis (HAS) was performed using Crystal Explorer17.5 [23]. The calculated Hirshfeld surface for L1 A and L1 B is depicted in **Figure 2(a)** and **Figure 2(b)**, respectively and have previously been reported as preliminary data to confirm the intermediate organic ligands [40]. The left Figures exhibit intramolecular mutual constellation as 3D Hirshfeld surfaces. The *de* (distance from the surface to the outermost nucleus) and *di* (distance from the surface to the inner closest nucleus) surfaces are illustrated in **Figure 2**, with the red spots representing the points of short intermolecular distances and blue area representing those of long intermolecular distance. The combination of *di* and *de* on a finger print plot (**Figure 2**) provides more information about all the contacts in the molecule. The Hirshfeld surface index map helps to analyze molecular contacts by colour code. The blue indicates low intensity contacts points, while the gray area represents the entire plot. For L1, the A's(aliphatic)N-H and O=C(carbonyl) can interact easily with the following atom-atom percent interaction; H-H = 39.2%, H-O = 8.2%, O-H = 5.7%, N-H = 9.5%, and N-C = 6.2%, while the B's (aliphatic)N-H and proton donors (aromatic)tend to interact strongly with the following atom-atom constitution percentage: H-H = 34.2%, H-O = 2.5%, O-H = 6.4%, C-C = 8.8%, and N-C = 9.0.

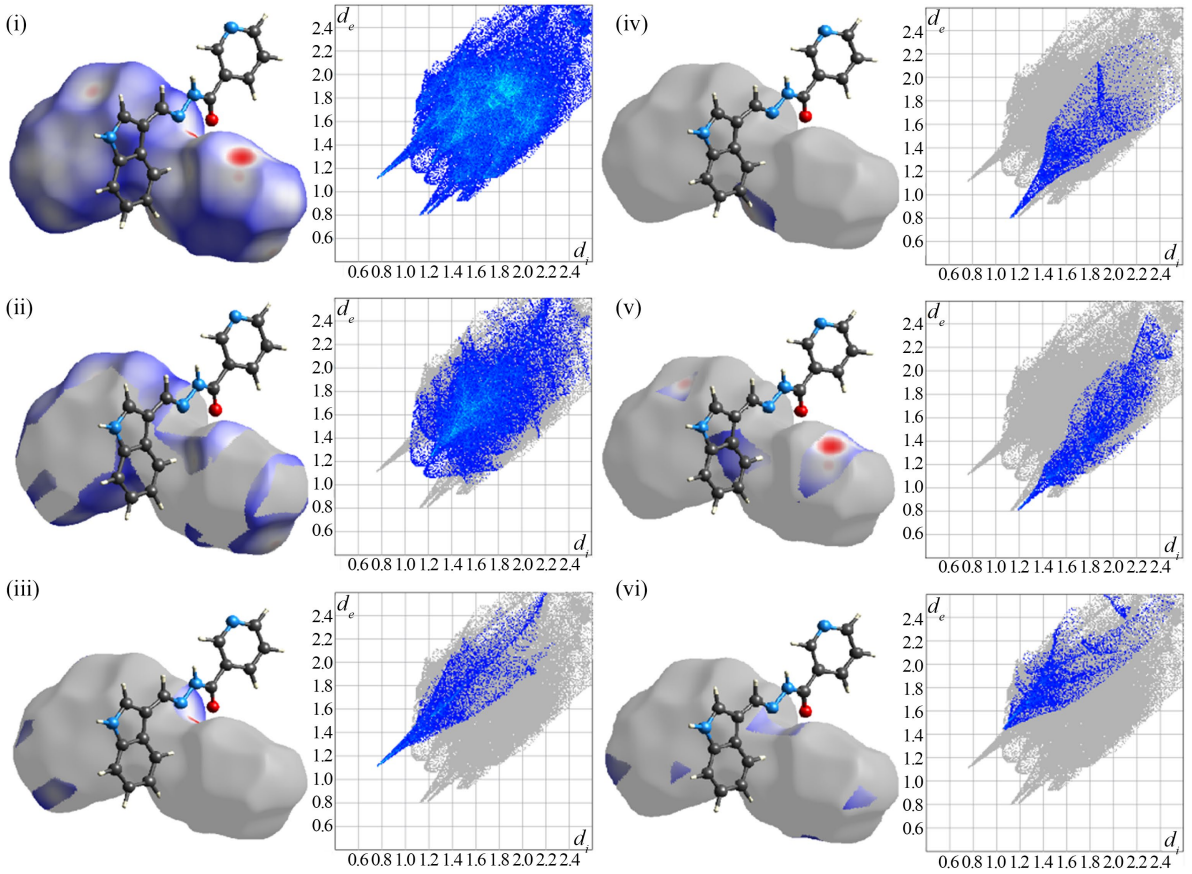

(a)

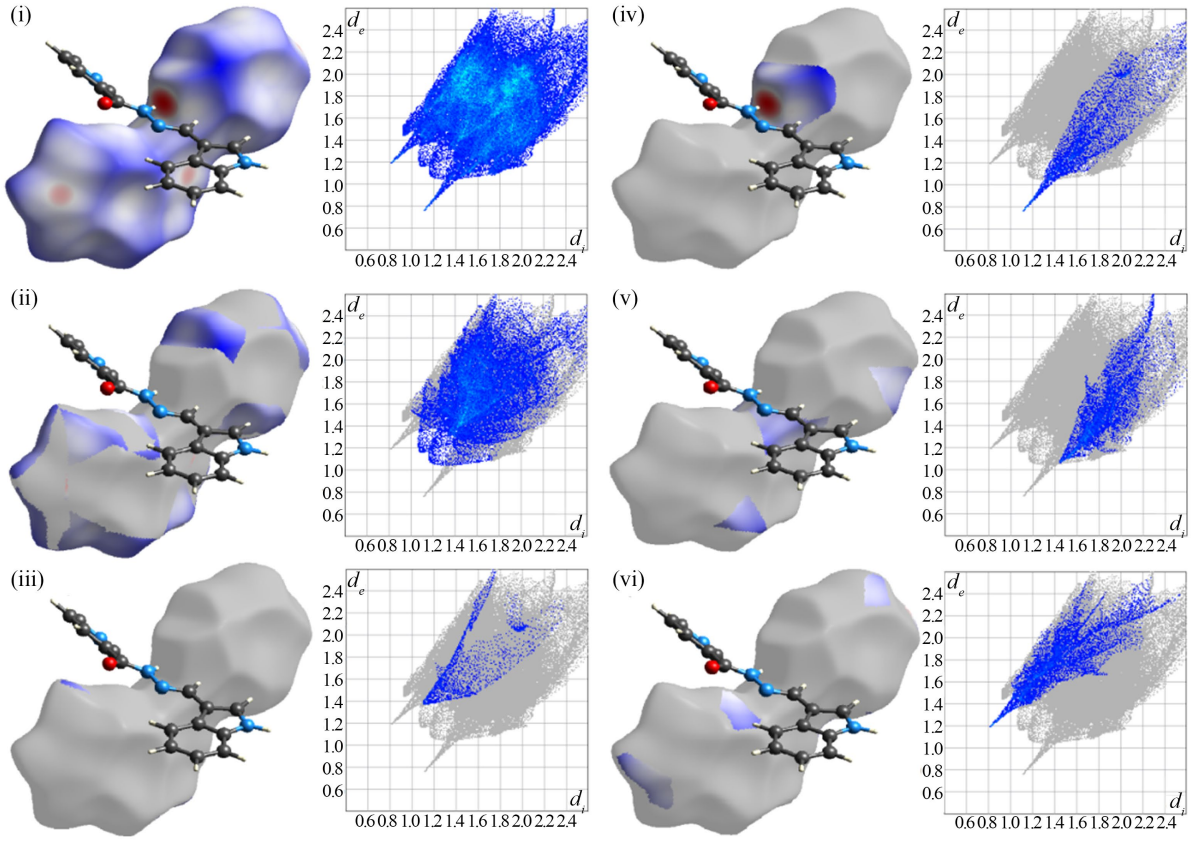

(b)

Figure 2. Hirshfeld surface fingerprint plots for the molecule L1 (a) A and (b) B.

3.6. Density Functional Theory Calculations

3.6.1. Geometry Optimization

Good quality single crystals of zinc (II) and copper (II) complexes suitable for X-ray analysis could not be obtained after repeated trials in different solvents. In order to examine the properties of the ligand and its metal(II) complexes, theoretical studies using DFT with the help of Gauss View 60.16 and Gaussian 09 suite of programme were carried. **Figure 3** depicts the optimized geometrical structures of the synthesized ligand and its metal (II) complexes.

This optimization was necessary gain the better insight on the structural features of the complexes. For the zinc complex, the Zn-O, and Zn-N bond lengths are 1.8984 and 1.9385 Å respectively. The C-N bond lengths are in the range of 1.2707 - 1.3867 Å. The O-Zn-O, N-Zn-N, O-Zn-N and N-Zn-O bond angles are 122.700˚, 121.080˚, 117.640˚ and 117.70˚ respectively. For the nickel (II) complex, the Ni-O bond lengths are in the range of 1.8123 - 1.8194 Å while the Ni-O bond lengths are in the range of 1.8270 - 1.8498 Å. The N-Ni-N and O-Ni-O bond angles are 91.124 and 70.7437 Å respectively. These bond lengths and bond angles are in line with previously reported results having similar ligands [42] [43].

Tables 2-4 contained some important quantum chemistry characteristics that have been taken into consideration with respects to the study compounds.

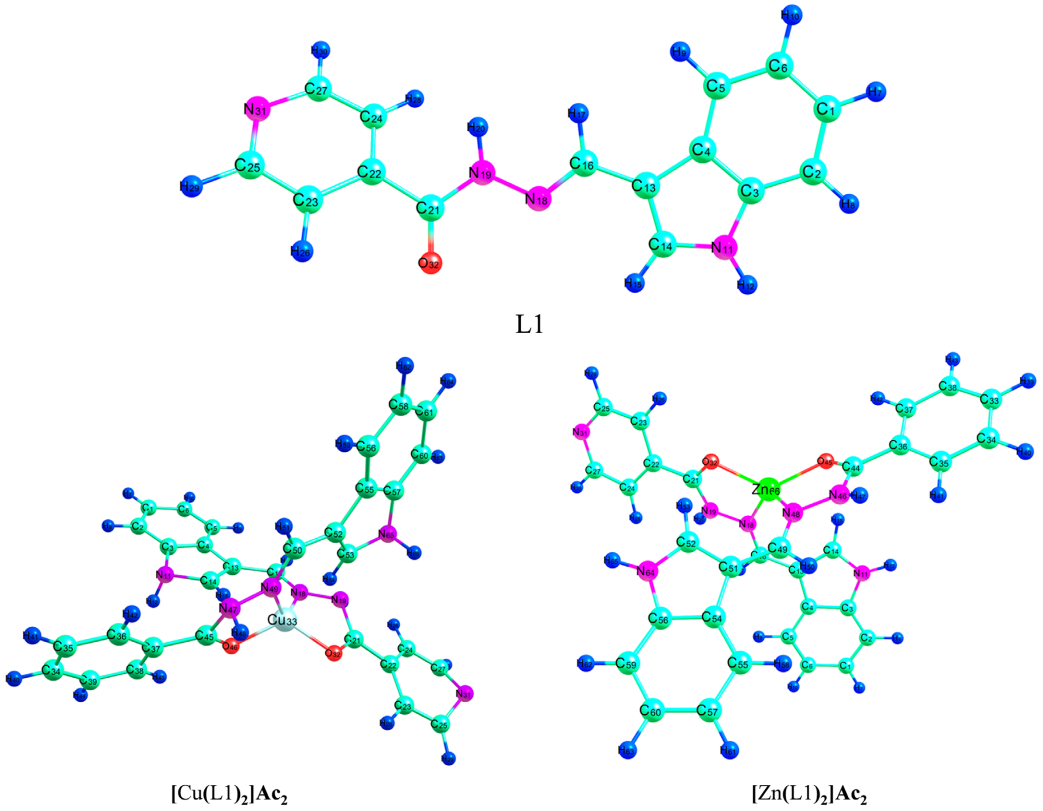

Figure 3. Optimized geometrical structure of L1 and its metal (II) complexes.

3.6.2. Frontier Molecular Orbital (FMO)

The HOMO, LUMO values were related to the ionization potential (IP) and electron affinity (EA) of the studied compounds by invoking Koopmans' approximation [41]. Global reactivity descriptors like IP, EA, electronegativity index (X), hardness (η), softness (σ), chemical potential (μ) and electrophilicity index (ω) were calculated for the for the ligand and its metal(II) complexes and summarized in **Table 3**.

The HOMO, LUMO, energy gap and the global quantum reactivity parameters computed were calculated and predicted at DFT/ωB97XD with 6-311G++(d, p) basis set. The results revealed that the ligand L1, and its metal(II) complexes possess the potential sites available to either give or accept electrons. Theoretically calculated energy gap for L1, $[Cu(L1)_2]Ac_2$ and $[Zn(L1)_2]Ac_2$ complexes were 5.9802 eV, 5.9773 eV and 6.6932 eV respectively. From this frontier molecular energy gap calculations, these compounds exhibit more chemical reactivity at this functional. These results were found to correlate with the biological activity of receptor 5e2c and its respective binding affinity for each of the compounds. In addition to the HOMO, LUMO and the energy gap, some important global relativity presented in **Table 3** were calculated with the aid of specific expression and equations in literatures [42]. The electrophilicity index of 24.0572 eV, 157.5885 eV and 158.0035 eV for L1, $[Cu(L1)_2]Ac_2$ and $[Zn(L1)_2]Ac_2$ respectively were obtained. Generally, electrophilicity index is an important parameter that helps in

affirming the toxicity of molecules by quantifying the biological activity of drug–receptor interaction. Figure 4 shows the electron delocalization along the molecules. The results further revealed that the HOMO was highly localized at the central metal atoms in the Cu(II) and Zn(II) complexes with LUMO distributed evenly on the entire complexes.

Table 3. HOMO, LUMO, Energy gap and global quantum descriptors reactivity of ligand (L1) and its metal (II) complexes at DFT/*ω*B97XD with 6-311G++ (d,p).

Parameters	L1	$[Cu(L1)_2]Ac_2$	$[Zn(L1)_2]Ac_2$
LUMO/eV	1.0212	7.2807	−6.3707
$E_{HOMO} - E_{LUMO}$ gap (eV)	5.9802	5.9773	6.6932
Electrophilicity index (ω)	24.0572	157.5885	158.0035
Electronegativity (χ)	4.0114	10.2693	−9.7173
Chemical potential (μ)	4.0114	10.2693	9.7173
Global hardness (η)	2.9901	2.9886	3.3466

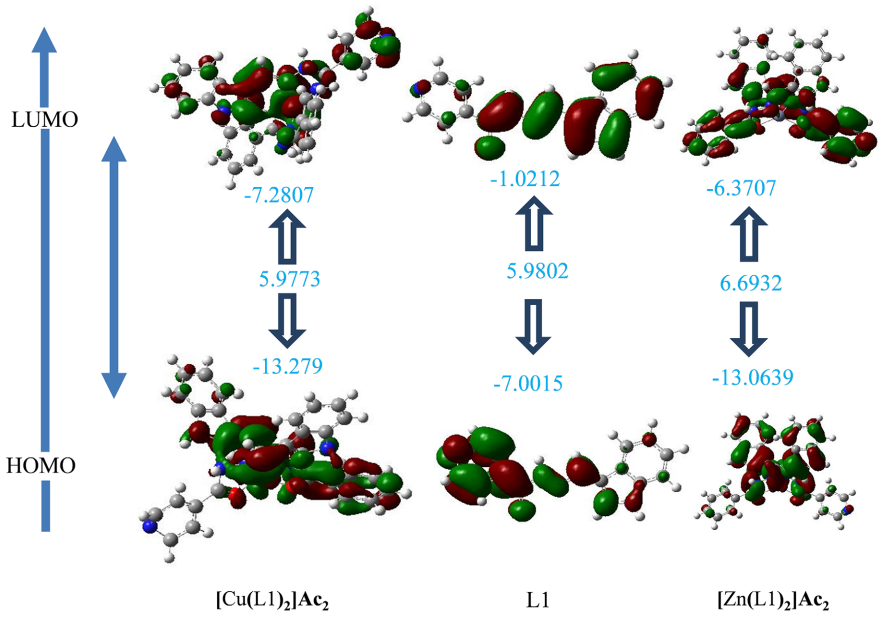

Figure 4. Pictorial representation of HOMO, LUMO and Energy gap of L1 and its metal(II) complexes.

3.6.3. Natural Bond Orbital (NBO) Study

The natural bond orbital analysis was performed with the zinc(II) and copper(II) complexes using DFT/wB97XD with 6-311G++ level of theory to give clarity of charge transfer, delocalization of electron density and energy of interaction in the molecules by considering core, valance and Rydberg sub-shells. The second order perturbation energies with intramolecular hyper conjugative interactions of L1, metal(II) complexes that result in the intermolecular charge transfer thereby affecting the stability of the of molecules under investigation are presented in Table 4. These results showed that the interactions with the highest second order per-

turbation energy for the delocalization of electrons from $\pi^* \rightarrow \sigma^*$ in the $[Cu(L1)_2]Ac_2$ complex with stabilization energies of 3224.53, 786.79, 477.29, 177.45 and 148.76 kcal/mol respectively, are due to the conjugative interactions. In the same vein, the intra- charge transfer within the L1 was delocalized within $\pi^* \rightarrow \pi^*$ with stabilization energies of 303.92, 213.47 kcal/mol, $\pi^* \rightarrow \sigma^*$ with energies of 194.82, 184.71 and 168.71 as in Table 4. The $[Zn(L1)_2]Ac_2$ complex inter-charge transfer had higher stabilization energies of 7512.22, 873.73, 782.47 and 603.49 kcal/mol for $\sigma^* \rightarrow \sigma^*$ transition whereas, $\pi^* \rightarrow \pi^*$ transition had energy of 308.61 kcal/mol. It is important to mention here that $\sigma^* \rightarrow \sigma^*$ had higher average stabilization energy which implies stronger interactions at this transition.

Table 4. Donor, Acceptor and second order stabilization energies of L1, $[Cu(L1)_2]Ac_2$ and $[Zn(L1)_2]Ac_2$ calculated with wB97XD.

Compounds	Donor (i)	Acceptor (j)	$E^{(2)}$ (kcal/mol)	E(j)-(i) (a.u)	F(i,j) (a.u)
L1	π^*C_{13} - C_{14}	π^*C_1 - C_2	303.92	0.02	0.098
	π^*C_{13}- C_{14}	π^*C_5 - C_6	213.47	0.02	0.097
	π^*C_{21} - C_{22}	σ^*C_{21} - C_{22}	194.82	0.57	0.670
$[Cu(L1)_2]Ac_2$	π^*C_{25} - N_{31}	σ^* C_{52} - C_{55}	3224.53	0.17	2.138
	π^*C_{25}- N_{31}	σ^*C_{52} - C_{53}	786.79	0.46	1.756
	π^*C_{25} - N_{31}	σ^*C_{50} - H_{51}	477.29	0.52	1.375
$[Zn(L1)_2]Ac_2$	σC_1 - C_7	σ^*N_{18} - N_{19}	7512.22	0.01	0.272
	σC_{21} - C_{32}	σ^*N_{18} - N_{19}	873.73	0.48	0.580
	σN_{19} - C_{21}	σ^*N_{18} - N_{19}	782.47	0.18	0.340

3.6.4. Density of States Study

The total density of state (TDOS) map, partial density of state (PDOS) map and the overlap population DOS (OPDOS) map of the three studied compounds were plotted with the help of multifunctional wavefunction analyzer to investigate the major contribution of each set of molecular orbitals [43]. The energy values of these compounds at the bonding molecular region are 17.00 a.u, 4.00 a.u and 3.00 a.u for carbon, hydrogen and nitrogen respectively, while other elements oxygen and zinc peaks were not intense. Carbon atoms were also observed to have the highest values at the antibonding region. For the complex $[Cu(L1)_2]Ac_2$, carbon was seen to have the highest and lowest values at 16.89 a.u and 12.28 a.u respectively. The hydrogen highest peak is seen at the band gap region with a value 3.06 at the antibonding region. For the ligand L1, the highest and lowest values of carbon are 9.50 a.u and 5.00 a.u, while nitrogen had 3.00 a.u heights and the hydrogen 2.00 a.u peak mean the oxygen atom was bond pronounced. From this comparative study, hydrogen was observed to have the highest peak at both bonding and the antibonding molecular regions, in each of the studied compounds. The other atomic contributions are negligible due to poor overlapping in orbital phase as their peaks are not intense. It is important to point out here that DOS spectral curves are useful in describing the electronic structures of compounds.

3.6.5. Quantum Theory of Atoms in Molecules (QTAIM) Study

The topology properties of the ligand and its metal (II) complexes were computed with the aid of multifunctional wave functional analyzer [44] and the results are summarized in Table 5, while Figure 5 depicts the critical bonds and the respective interactions in the zinc(II) and copper(II) complexes. From the results it is observed that $[Cu(L1)_2]Ac_2$ complex has two intermolecular interactions whereas, $[Zn(L1)_2]Ac_2$ complex has four interactions. The results in Table 5 clearly point out that, $[Cu(L1)_2]Ac_2$ complex have the highest density of electrons at the respective bond critical points. The highest values are observed from the intermolecular interaction of Zn_{66} - O_{45}-----H_{15} with the ρ(r) value of 0.847 eV and the other bond Zn_{66} - O_{32}-----H_{58} with the calculated value of 0.797 eV. It is very pertinent to mention here that, all the interactions observed in CuL1 complex are positive thereby indicating electrostatic interactions. Furthermore, all the data presented herein indicates that, the interactions are weak since their densities of electrons and Laplacian are positive. The interactions in the $[Cu(L1)_2]Ac_2$ complex are observed to have ρ(r) value of 0.05 eV. The strength of any pair of interacting atoms is reflected by the electron density at the corresponding bond critical point. The $[Zn(L1)_2]Ac_2$ complex is observed to have four interactions with all having negative values of H(r) and shorter density of electrons ρ(r) which is a clear indication that the interactions were very strong. The observable interactions observed here areN_{18}-----H_{53} – C_{52}, N_{11} – H_{12}-----C_{37}, O_{45} –H_{15}-----C_{14} and N_{18} – C_{66}-----O_{32} with electron densities of 0.124, 0.383, 0.241 and 0.105 eV respectively resulting to the negative values of H(r) which is an indication of the strength of the bonds. The G(r), K(r) and V(r) parameters computed were to further reveal the nature and the strength of the bonds observed in interactions.

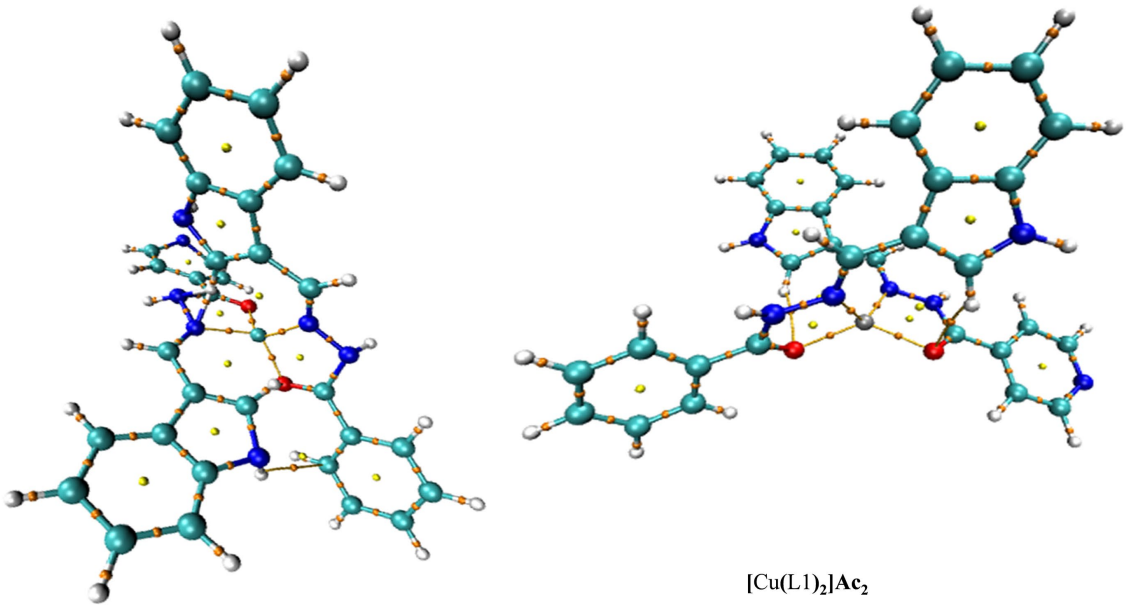

Figure 5. Critical bonds and the respective interactions in the $[Zn(L1)_2]Ac_2$ and $[Cu(L1)_2]Ac_2$ complexes.

Table 5. Bond formation in the quantum theory of atoms in molecule for $[Cu(L1)_2]Ac_2$ and $[Zn(L1)_2]Ac_2$ complexes.

Compound	Bond	$\rho(r)$	$\nabla\rho(r)$	G(r)	K(r)	V(r)	H(r)
$[Cu(L1)_2]Ac_2$	Zn_{66} - O_{45}-----H_{15}	0.847	0.293	0.609	−0.123	−0.487	0.123
	Zn_{66} - O_{32}-----H_{58}	0.797	0.275	0.574	−0.115	−0.459	0.115
$[Zn(L1)_2]Ac_2$	N_{18}-----H_{53} - C_{52}	0.124	0.268	0.129	0.616	−0.190	−0.616
	N_{11} - H_{12}-----C_{37}	0.383	0.279	0.553	−0.146	−0.406	0.146
	O_{45} - H_{15}-----C_{14}	0.241	−0.495	0.889	0.213	−0.3016	−0.213
	N_{18} - C_{66}-----O_{32}	0.105	0.666	0.175	0.911	−0.185	−0.911

3.7. Anti-Tuberculosis Study

The hydrazone ligand L1, its copper(II) and zinc(II) complexes were evaluated against *Mycobaterium tuberculosis* H37Rv strain (*ATCC 27294*), using the Alamer blue assay. Pyrazinamide and isoniazid were used as standard reference. The results are as presented in Table 6.

Table 6. The *in vitro* activity of the ligand and its metal complexes against *M. Tuberculosis* H37Rv strain (*ATCC 27294*).

1) Compound	2) MIC (μg/mL) ± SD
3) $C_{15}H_{12}N_4O$	4) 6.25 ± 0.72
5) $[Cu(L1)_2]Ac_2$	6) 1.25 ± 0.13
7) $[Zn(L1)_2]Ac_2$	8) 3.12 ± 0.34
9) Pyrazinamide	10) 3.12 ± 0.34
11) Isoniazid	12) 3.12 ± 0.34

*Values expressed are mean ± SD of three parallel measurements.

The copper(II) complex with MIC 1.25 ± 0.13 μg/mL exhibited the highest anti-tuberculosis activity compared to the zinc (II) complex with MIC value of 3.2 ± 0.34 μg/mL and all standards as shown in Table 6. The ligand with MIC value 6.25 ± 0.72 μM exhibited the least activity compared to its metal complexes. This may be attributed to the reduced polarity of the central metals(II) ions which partially share their positive charges with the donor groups as well as the possible π-electron delocalization within the entire chelating ring system formed during coordination. This enhances the lipophilic character of the central metal atoms/ions, thereby increasing their hydrophobic character and favoring their ability to permeate the lipid layers of the cell membrane as explained by the Tweedy's chelation theory [45]. Overall, the results showed higher activity of the metal (II) complexes against *M. tuberculosis* as compared to ligand.

3.8. Molecular Docking Study

The comparative molecular docking study was employed to study the drug delivery of L1, $[Cu(L1)_2]Ac_2$, and $[Zn(L1)_2]Ac_2$. They were docked in the active site of

the protein 5e2c which is a mycobacterium. To further understand the suitability of L1, Cu (II) and Zn(II) complexes as potential tuberculosis drug candidates, molecular docking studies was performed on the optimized structures of the studied compounds and the bioactivity score detected based on the interaction with the selected receptor protein and the standard drug. The binding affinities were monitored in kcal/mol unit for a negative score. The 3D crystallographic structures of the receptor molecules chosen for docking studies were achieved from the Protein Data Bank (PDB) [46]. The receptor proteins were prepared by removing water molecule, adding explicit hydrogen and charges and correction of deformation in amino acid sequence. The active sites of the receptor protein were predicted and defined based on the interaction of the crystallographic ligand with the receptor molecules respectively as visualized with the discovery studio visualizer and pymol visualizer. Protein preparation which allowed for purification of the protein for proper docking was done using bio *via* Discovery studio; the selected proteins were dock with the ligand using auto dock tools with the help of vina command. Visualization of the receptor and ligand interaction shown in **Figure 6** was done with the help of discovery studio. The result for molecular docking showed an excellent interaction between the L1, its Cu(II), Zn(II) complexes and the selected receptor protein. The docking result generated 9 modes with average binding affinity computed, the docking result was compared to the standard drug Isoniazid and the result showed the trend $[Cu(L1)_2]Ac_2$ > $[Zn(L1)_2]Ac_2$ > L1 > isoniazid with respective average binding affinities of −8.3, −7.8, −6.3 and −4.2 accordingly. A linear correlation was found between the docking scores of the test compounds and the corresponding reactivity values, where the active compounds showed a high docking score, while the compound with higher reactivity values showed a lower docking score. These results are presented in **Table 7**. From the visualization with discovery studio, it was observed that $[Cu(L1)_2]Ac_2$ and L1 had three conventional hydrogen bond interactions. The amino acids observed with this hydrogen bond interaction were *B: SER 25: HG* and *B: THR 103 HN* while four hydrogen bonds were observed in $[Zn(L1)_2]Ac_2$ complex from A: *THR:103: HG1* whereas no hydrogen bond was found in the isoniazid. From this visualization it was observed that hydrogen bond was not the only type of interaction found in the studied compounds but other interaction like *pi -sigma*, *pi – pi* stacked, *pi*-alkyl and lost steric interaction were observed. Hydrogen bond determines the activeness of a potential drug candidate and hence the studied compounds having the highest binding affinity with much number of hydrogen atoms implies better tuberculosis drug candidate.

Table 7. Modes, binding and average binding affinities of L1 and its metal complexes in kcal/mol.

Modes	L1	$[Zn(L1)_2]Ac_2$	$[Cu(L1)_2]Ac_2$	Isoniazid
1	−6.7	−8.3	−9.0	−4.4
2	−6.5	−8.1	−8.7	−4.4
3	−6.4	−8.0	−8.7	−4.4

Continued

4	−6.3	−8.0	−8.6	−4.3
5	−6.2	−7.9	−8.3	−4.3
6	−6.2	−7.9	−8.2	−4.2
7	−6.2	−7.8	−8.1	−4.1
8	−6.2	−7.6	−7.9	−4.0
9	−6.0	−7.4	−7.6	−3.9
Average binding affinity/kcal/mol	−6.3	−7.8	−8.3	−4.2

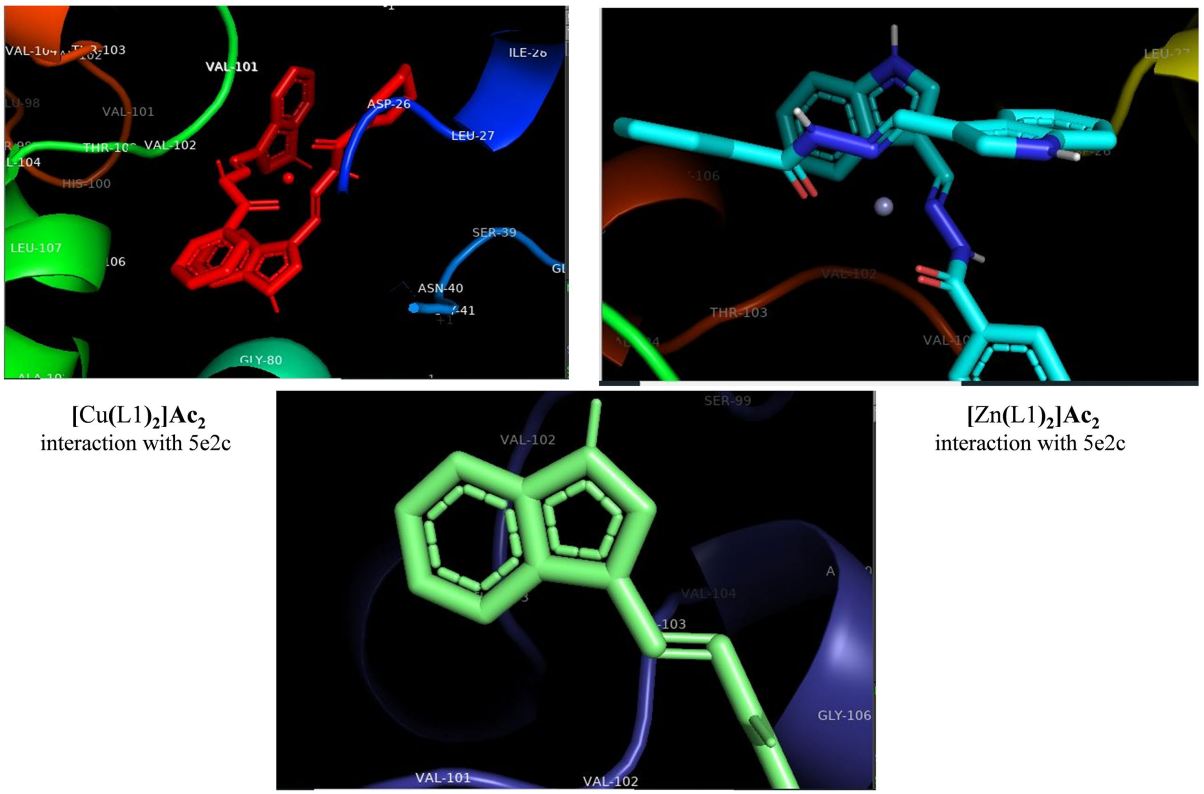

$[Cu(L1)_2]Ac_2$ interaction with 5e2c

$[Zn(L1)_2]Ac_2$ interaction with 5e2c

L1 interaction with 5e2c

Figure 6. Interaction network between the complexes and *M. tuberculosis* protein structures.

4. Conclusion

A nicotinic derived Schiff base ligand and its Cu (II) and Zn (II) complexes were successfully synthesized with bidentate N and O donor Schiff base ligand derived from nicotinic acid hydrazide. Their chemical structures were confirmed using several spectroscopic tools including IR, ^{1}H-NMR and XRD techniques. Further elucidation for the metalation of the synthesized Schiff base was performed through DFT and calculation of some chemical parameters. It was revealed that the Schiff base ligand behaved in a bidentate manner in all metal complexes through the azomethine nitrogen and carbonyl group of nicotine moiety. The *In vitro* antibacterial activities of the compounds were studied and demonstrate that the complexes formation increased their antibacterial activities toward *M. tuber-*

culosis. The molecular docking studies revealed favorable average binding energies for the prepared compound in the order $[Cu(L1)_2]Ac_2$ > $[Zn(L1)_2]Ac_2$ > L1 > isoniazid, the reference drug.

Supplementary Materials

The supplementary crystallographic data, CCDC Deposition Number 2124184 for L1 can be obtained free of charge via http://www.ccdc.cam.ac.uk/ conts/ retrieving.html (or from the Cambridge Crystallographic Data Centre, 12, Union Road, Cambridge CB21EZ, UK; fax: +44 1223 336033).

Acknowledgements

This work was also supported by a Grant-in-Aid for Scientific Research (A) KAKENHI (20H00336).

Author Contributions

Emmanuel N. Nfor, Takashiro Akitsu: Conceptualization, design, supervision, and editing. **Ebobobi Ebotagbo, Evans Mainsah:** Analysis, Investigation and manuscript first draft, **Emmanuel N. Nfor, Natsuki Katsuunmi, Takashiro Akitsu:** Validation, Investigation, Analysis, Writing, Review, Editing and manuscript final draft, **Gwendoline M. Toh Boyo:** Analysis, and writing, **Offiong Offiong, Shintaro Suda:** Data curation, analysis and writing, **Terkumbur Gber:** Analysis, and writing, **Emmanuel N. Nfor:** Supervision, Review and editing, **Takashiro Akitsu:** Methodology, editing, and resources. All authors have read and agreed to the published version of the manuscript.

Conflicts of Interest

The authors declare no conflict of interest.

References

[1] Levin-Reisman, I., Ronin, I., Gefen, O., Braniss, I., Shoresh, N. and Balaban, N.Q. (2017) Antibiotic Tolerance Facilitates the Evolution of Resistance. *Science*, **355**, 826-830. https://doi.org/10.1126/science.aaj2191

[2] Wang, L., Battini, N., Bheemanaboina, R.R.Y., Zhang, S. and Zhou, C. (2019) Design and Synthesis of Aminothiazolyl Norfloxacin Analogues as Potential Antimicrobial Agents and Their Biological Evaluation. *European Journal of Medicinal Chemistry*, **167**, 105-123. https://doi.org/10.1016/j.ejmech.2019.01.072

[3] Sprenger, M. and Fukuda, K. (2016) New Mechanisms, New Worries. *Science*, **351**, 1263-1264. https://doi.org/10.1126/science.aad9450

[4] Brown, E.D. and Wright, G.D. (2016) Antibacterial Drug Discovery in the Resistance Era. *Nature*, **529**, 336-343. https://doi.org/10.1038/nature17042

[5] Silver, L.L. (2011) Challenges of Antibacterial Discovery. *Clinical Microbiology Reviews*, **24**, 71-109. https://doi.org/10.1128/cmr.00030-10

[6] Coates, A., Hu, Y., Bax, R. and Page, C. (2002) The Future Challenges Facing the Development of New Antimicrobial Drugs. *Nature Reviews Drug Discovery*, **1**, 895-

910. https://doi.org/10.1038/nrd940

[7] Oladipo, S.D., Olotu, F.A., Soliman, M., Mocktar, C. and Omondi, B. (2020) Formamidine-Based Thiuram Disulfides: Synthesis, Structural Characterization, Biological Studies, and Preliminary Cheminformatics Evaluation. *Journal of Molecular Structure*, **1219**, Article ID: 128553. https://doi.org/10.1016/j.molstruc.2020.128553

[8] Esteban, J. and García-Coca, M. (2018) Mycobacterium Biofilms. *Frontiers in Microbiology*, **8**, Article 2651. https://doi.org/10.3389/fmicb.2017.02651

[9] Philley, J.V. and Griffith, D.E. (2015) Treatment of Slowly Growing Mycobacteria. *Clinics in Chest Medicine*, **36**, 79-90. https://doi.org/10.1016/j.ccm.2014.10.005

[10] WHO (2021) Tuberculosis. Global Tuberculosis Report 2019. https://www.who.int/health-topics/tuberculosis#tab=tab_1

[11] Roat-Malone, R.M. (2002) Bioinorganic Chemistry: A Short Course. Wiley, 348 p. https://doi.org/10.1002/0471265330

[12] Bertini, I., Gray, H.B., Stiefel, E.I. and Valentine, J.S. (2007) Biological Inorganic Chemistry: Structure and Reactivity. University Science Books, 73 p.

[13] Berg, J.M. and Godwin, H.A. (1997) Lessons from Zinc-Binding Peptides. *Annual Review of Biophysics and Biomolecular Structure*, **26**, 357-371. https://doi.org/10.1146/annurev.biophys.26.1.357

[14] Jernigan, R., Raghunathan, G. and Bahar, I. (1994) Characterization of Interactions and Metal Ion Binding Sites in Proteins. *Current Opinion in Structural Biology*, **4**, 256-263. https://doi.org/10.1016/s0959-440x(94)90317-4

[15] Sadler, P.J. (1991) Inorganic Chemistry and Drug Design. In: Emeleua, H.J. and Sharpe, A.G., Eds., *Advances in Inorganic Chemistry*, Elsevier, 1-48. https://doi.org/10.1016/s0898-8838(08)60035-5

[16] Fricker, S.P. (2007) Metal Based Drugs: From Serendipity to Design. *Dalton Transactions*, **43**, 4903-4917. https://doi.org/10.1039/b705551j

[17] Nakahata, D.H., de Paiva, R.E.F., Lustri, W.R. and Corbi, P.P. (2020) Sulfonamide-Containing Copper(II) Complexes: New Insights on Biophysical Interactions and Antibacterial Activities. *New Journal of Chemistry*, **44**, 17236-17244. https://doi.org/10.1039/d0nj01889a

[18] Toh-Boyo, G.M., Njong, R.N., Babette, E.M. and Nfor, E.N. (2021) Synthesis, Spectroscopic, Molecular Modeling and Anti-Fungal Studies of Some Divalent Metal Complexes of 4-Hydroxyacetophenone Isonicotinoyl Hydrazone. *Open Journal of Inorganic Chemistry*, **11**, 95-109. https://doi.org/10.4236/ojic.2021.113007

[19] Nfor, E.N., Husian, A., Majoumo-Mbe, F., Njah, I.N., Offiong, O.E. and Bourne, S.A. (2013) Synthesis, Crystal Structure and Antifungal Activity of a Ni(II) Complex of a New Hydrazone Derived from Antihypertensive Drug Hydralazine Hydrochloride. *Polyhedron*, **63**, 207-213. https://doi.org/10.1016/j.poly.2013.07.028

[20] Mikwa, C.C., Toh-Boyo, G.M., Njong, R.N., Ndoye, B.N., Ndamyabera, C.A., Katsuumi, N., *et al.* (2022) Bivalent Metal Complexes of a Novel Modified Nicotinic Acid Hydrazide Drug: Synthesis, Characterization, and Anti-Tubercular Studies. *European Journal of Chemistry*, **13**, 63-68. https://doi.org/10.5155/eurjchem.13.1.63-68.2183

[21] Watat, M.L., Chi, J.S., Asanji, C.E. and Nfor, E.N. (2022) Synthesis, Characterization, Computational and Antibacterial Studies of Novel Dopamine-Based Derivatives. *International Journal of Organic Chemistry*, **12**, 40-52. https://doi.org/10.4236/ijoc.2022.121004

[22] Sheldrick, G.M. (2015) Crystal Structure Refinement with *SHELXL*. *Acta Crystallographica Section C Structural Chemistry*, **71**, 3-8. https://doi.org/10.1107/s2053229614024218

[23] Wolff, S.K., Grimwood, D.J., McKinnon, J.J., Jayatilaka, D. and Spackman, M.A. (2017) Crystal Explorer 17.5. University of Western Australia.

[24] Frisch, M.J., Trucks, G.W., Schlegel, H.B., Scuseria Robb, M.A., *et al.* (2009) Fox, Gaussian 09. Gaussian, Inc.

[25] Rajan, R.V., Gowri, S., Manopradha, N., Leenaraj, D.R., Joy, L.K. and Sajan, D. (2019) Growth, Structural, Third Order Nonlinear Optical Properties, Dielectric Properties, Conductivity Mechanisms and Spectroscopic Characterization of a Luminescent Material Trans-Diaqua-Bis(Pyridine-2-Carboxylato)-Cobalt(II) Dihydrate for Optoelectronic Applications. *Optics & Laser Technology*, **119**, Article ID: 105664. https://doi.org/10.1016/j.optlastec.2019.105664

[26] Lu, T. and Chen, F. (2011) Multiwfn: A Multifunctional Wavefunction Analyzer. *Journal of Computational Chemistry*, **33**, 580-592. https://doi.org/10.1002/jcc.22885

[27] Canetti, G., Froman, S., Grosset, J., Hauduroy, P., Miloslava, L., Mahler, H.T., Gertrud, M., Mitchison, D.A. and Šula, L. (1963) Mycobacteria: Laboratory Methods for Testing Drug Sensitivity and Resistance. *Bulletin of the World Health Organization*, **29**, 565-578.

[28] Franzblau, S.G., Witzig, R.S., McLaughlin, J.C., Torres, P., Madico, G., Hernandez, A., *et al.* (1998) Rapid, Low-Technology MIC Determination with Clinical *Mycobacterium Tuberculosis* Isolates by Using the Microplate Alamar Blue Assay. *Journal of Clinical Microbiology*, **36**, 362-366. https://doi.org/10.1128/jcm.36.2.362-366.1998

[29] Tan, B. and Vanitha, J. (2004) Immunomodulatory and Antimicrobial Effects of Some Traditional Chinese Medicinal Herbs: A Review. *Current Medicinal Chemistry*, **11**, 1423-1430. https://doi.org/10.2174/0929867043365161

[30] Reis, H.T., Clar, M.S.J. and Holmes, K. (2004) Perceived Partner Responsiveness as an Organizing Construct in the Study of Intimacy and Closeness. In: Mashek, D.J. and Aron, A.P., Eds., *Handbook of Closeness and Intimacy*, Lawrence Erlbaum Associates Publishers, 201-225.

[31] Lourenço, M.C.S., Souza, M.V.N.D., Pinheiro, A.C., Ferreira, M.D.L., Gonçalves, R.S.B., Nogueira, T.C.M., *et al.* (2007) Evaluation of Anti-Tubercular Activity of Nicotinic and Isoniazid Analogues. *Arkivoc*, **2007**, 181-191. https://doi.org/10.3998/ark.5550190.0008.f18

[32] Huey, R., Morris, G.M. and Forli, S. (2012) Using AutoDock 4 and AutoDockvina with AutoDockTools: A Tutorial. The Scripps Research Institute Molecular Graphics Laboratory10550, 92037.

[33] Song, C., Tian, Z., Wang, C., Shi, R. and Liu, J. (2020) Growth Behavior and Properties of $(HF)_{1-16}$ Clusters. *Structural Chemistry*, **32**, 395-403. https://doi.org/10.1007/s11224-020-01637-2

[34] Li, M., Wei, Y., Zhang, G., Wang, F., Li, M. and Soleymanabadi, H. (2020) A DFT Study on the Detection of Isoniazid Drug by Pristine, Si and Al Doped C_{70} Fullerenes. *Physica E*: *Low-Dimensional Systems and Nanostructures*, **118**, Article ID: 113878. https://doi.org/10.1016/j.physe.2019.113878

[35] Favila, A., Gallo, M. and Glossman-Mitnik, D. (2007) CHIH-DFT Determination of the Molecular Structure Infrared Spectra, UV Spectra and Chemical Reactivity of Three Antitubercular Compounds: Rifampicin, Isoniazid and Pyrazinamide. *Journal of Molecular Modeling*, **13**, 505-518. https://doi.org/10.1007/s00894-007-0170-2

[36] Berman, H.M., Battistuz, T., Bhat, T.N., Bluhm, W.F., Bourne, P.E., Burkhardt, K., *et al.* (2002) The Protein Data Bank. *Acta Crystallographica Section D Biological Crystallography*, **58**, 899-907. https://doi.org/10.1107/s0907444902003451

[37] N. Nfor, E., N. Esemu, S., A. Ayimele, G., A. Eno, E., Iniama, G.E. and Offiong, O.E. (2011) Synthesis, Stereochemistry and Antimicrobial Activity of Copper(II) and Nickel(II) Complexes of 4-Phenylsemicarbazones. *Bulletin of the Chemical Society of Ethiopia*, **25**, 361-370. https://doi.org/10.4314/bcse.v25i3.68668

[38] Offiong, O.E., Nfor, E., Ayi, A.A. and Martelli, S. (2000) Synthesis, Spectral and Cytotoxicity Studies of Palladium(II) and Platinum(II) Amino Acid Schiff Base Complexes. *Transition Metal Chemistry*, **25**, 369-373. https://doi.org/10.1023/a:1007055304150

[39] Nfor, E.N., Liu, W., Zuo, J., You, X. and Offiong, O.E. (2006) Di-μ-Acetato-Bis[(2-Acetylpyridine Thiosemicarbazonato)Zinc(II)]. *Acta Crystallographica Section C Crystal Structure Communications*, **62**, m211-m213. https://doi.org/10.1107/s0108270106009152

[40] Akitsu, T., Suda, S. and Katsuumi, N. (2021) Beyond the Scope of Each Computational Chemistry. *Edelweiss Chemical Science Journal*, **4**, 25-26. https://doi.org/10.33805/2641-7383.128

[41] Louis, H., Gber, T.E., Asogwa, F.C., Eno, E.A., Unimuke, T.O., Bassey, V.M., *et al.* (2022) Understanding the Lithiation Mechanisms of Pyrenetetrone-Based Carbonyl Compound as Cathode Material for Lithium-Ion Battery: Insight from First Principle Density Functional Theory. *Materials Chemistry and Physics*, **278**, Article ID: 125518. https://doi.org/10.1016/j.matchemphys.2021.125518

[42] Carpenter, J.E. and Weinhold, F. (1988) Analysis of the Geometry of the Hydroxymethyl Radical by the "Different Hybrids for Different Spins" Natural Bond Orbital Procedure. *Journal of Molecular Structure*: *Theochem*, **169**, 41-62. https://doi.org/10.1016/0166-1280(88)80248-3

[43] Khaliullin, R.Z., Bell, A.T. and Head-Gordon, M. (2008) Analysis of Charge Transfer Effects in Molecular Complexes Based on Absolutely Localized Molecular Orbitals. *The Journal of Chemical Physics*, **128**, Article ID: 184112. https://doi.org/10.1063/1.2912041

[44] Singh, R.N., Kumar, A., Tiwari, R.K. and Rawat, P. (2013) A Combined Experimental and Theoretical (DFT and AIM) Studies on Synthesis, Molecular Structure, Spectroscopic Properties and Multiple Interactions Analysis in a Novel Ethyl-4-[2-(Thiocarbamoyl)Hydrazinylidene]-3,5-Dimethyl-1H-Pyrrole-2-Carboxylate and Its Dimer. *Spectrochimica Acta Part A*: *Molecular and Biomolecular Spectroscopy*, **112**, 182-190. https://doi.org/10.1016/j.saa.2013.04.002

[45] Tweedy, B.G. (1964) Plant Extracts with Metal Ions as Potential Antimicrobial Agents. *Phytopathology*, **55**, 910-914.

[46] Chen, Y.Z. and Zhi, D.G. (2001) Ligand-Protein Inverse Docking and Its Potential Use in the Computer Search of Protein Targets of a Small Molecule. *Proteins*: *Structure*, *Function*, *and Genetics*, **43**, 217-226. https://doi.org/10.1002/1097-0134(20010501)43:2<217::aid-prot1032>3.0.co;2-g